10-1-2022

Evaluating brain damage in multiple sclerosis with simultaneous multi-angular-relaxometry of tissue

Biao Xiang

Jie Wen

Robert E Schmidt

Alexander L Sukstanskii

Daniel Mamah

See next page for additional authors

Authors

Biao Xiang, Jie Wen, Robert E Schmidt, Alexander L Sukstanskii, Daniel Mamah, Dmitriy A Yablonskiy, and Anne H Cross

RESEARCH ARTICLE

Evaluating brain damage in multiple sclerosis with simultaneous multi-angular-relaxometry of tissue

Biao Xiang[1], Jie Wen[1], Robert E. Schmidt[2], Alexander L. Sukstanskii[1], Daniel Mamah[3], Dmitriy A. Yablonskiy[1] & Anne H. Cross[4] (iD)

[1]Department of Radiology, Washington University, St. Louis, Missouri, 63110, USA
[2]Department of Pathology, Washington University, St. Louis, Missouri, 63110, USA
[3]Department of Psychiatry, Washington University, St. Louis, Missouri, 63110, USA
[4]Department of Neurology, Washington University, St. Louis, Missouri, 63110, USA

Correspondence

Anne H. Cross, Department of Neurology, Washington University, 660 South Euclid, Campus Box 8111, St. Louis, MO 63110, USA. Tel: +1 314 362 3293; Fax: +1 314 747 1345; E-mail: crossa@wustl.edu

Abstract

Objective: Multiple sclerosis (MS) is a common demyelinating central nervous system disease. MRI methods that can quantify myelin loss are needed for trials of putative remyelinating agents. Quantitative magnetization transfer MRI introduced the macromolecule proton fraction (MPF), which correlates with myelin concentration. We developed an alternative approach, Simultaneous-Multi-Angular-Relaxometry-of-Tissue (SMART) MRI, to generate MPF. Our objective was to test SMART-derived MPF metric as a potential imaging biomarker of demyelination. **Methods**: Twenty healthy control (HC), 11 relapsing–remitting MS (RRMS), 22 progressive MS (PMS), and one subject with a biopsied tumefactive demyelinating lesion were scanned at 3T using SMART MRI. SMART-derived MPF metric was determined in normal-appearing cortical gray matter (NAGM), normal-appearing subcortical white matter (NAWM), and demyelinating lesions. MPF metric was evaluated for correlations with physical and cognitive test scores. Comparisons were made between HC and MS and between MS subtypes. Furthermore, correlations were determined between MPF and neuropathology in the biopsied person. **Results**: SMART-derived MPF in NAGM and NAWM were lower in MS than HC ($p < 0.001$). MPF in NAGM, NAWM and lesions differentiated RRMS from PMS ($p < 0.01$, $p < 0.001$, $p < 0.001$, respectively), whereas lesion volumes did not. MPF in NAGM, NAWM and lesions correlated with the Expanded Disability Status Scale ($p < 0.01$, $p < 0.001$, $p < 0.001$, respectively) and nine-hole peg test ($p < 0.001$, $p < 0.001$, $p < 0.01$, respectively). MPF was lower in the histopathologically confirmed inflammatory demyelinating lesion than the contralateral NAWM and increased in the biopsied lesion over time, mirroring improved clinical performance. **Interpretation**: SMART-derived MPF metric holds potential as a quantitative imaging biomarker of demyelination and remyelination.

Introduction

Multiple Sclerosis (MS) is a common demyelinating disease of the central nervous system (CNS), affecting approximately 1 in 900 people in the United States.[1] MRI plays a critical role in MS diagnosis and disease monitoring[2–4] by detecting focal white matter lesions. However, standard clinical MRI correlates only modestly with disability and lacks specificity to MS pathology.[3,5,6]

Moreover, the normal-appearing white matter (NAWM) of MS brain is typically not truly normal. Gray matter demyelinating lesions are often widespread as well, but gray matter lesions are almost undetectable by conventional MR imaging.[7] Numerous studies have been devoted to the development and experimental validation of quantitative methods sensitive to myelin damage (the hallmark of MS neuropathology), primarily, by means of multi-exponential *T2* imaging of water trapped between myelin

layers, magnetization transfer (MT) and diffusion tensor imaging.[8]

One of these approaches, MT imaging, has been frequently used to estimate myelin damage.[9–11] MT studies use the concept of two cross-exchanging pools with a "free" (or liquid) pool consisting of highly mobile protons associated with intracellular and extracellular water with long *T2* (in the range 10–100 ms), and a "bound" pool consisting of less mobile protons with an ultrashort *T2* (less than 1 ms) associated with macromolecules and membranes in tissues. Loss of myelin leads to decreased concentration of macromolecules and a consequent decrease of the "bound" pool. Given its ultrashort *T2*, measuring signals directly from the "bound" pool has been challenging. However, using MT effects, the exchange between the pools allows indirect measurement of the "bound" pool's parameters.

Many MT studies use the magnetization transfer ratio (MTR) as a surrogate for myelin content.[11] However, traditional MTR depends on MRI pulse sequence parameters and does not provide the true macromolecule content. Quantitative magnetization transfer (qMT) can measure the fraction of bound protons versus total protons, the so called Macromolecule Proton Fraction (MPF)[12–20] which reflects myelin content.[21,22] While initially qMT has been limited by low resolution, high radio frequency energy deposition (especially, at magnetic fields 3 T and higher), and long acquisition times, new approaches have been proposed to overcome some of these constraints.[23,24]

Recently, we developed a technique for quantitative measurement of parameters characterizing MT effects without applying off-resonance radiofrequency pulses, which we call "Simultaneous Multi-Angular Relaxometry of Tissue" (SMART) MRI.[25] Similar to qMT, the SMART MRI metrics are sensitive to tissue macromolecule content and can measure MPF. To do this, the SMART method uses a gradient recalled echo (GRE) MRI and a model of GRE signal that derives cross-relaxation effects between "free" and "bound" proton pools. Because no MT pulses are used, the high radio frequency energy deposition associated with existing qMT approaches is eliminated. From a single protocol, this technique can generate quantitative MPF images, and additionally generates naturally co-registered quantitative images of longitudinal relaxation rate parameter ($R1 = 1/T1$) and spin density. Thus, SMART MRI has the potential to provide high resolution quantitative multi-parametric information regarding myelin content without high radio frequency energy deposition.

Here we report for the first time the application of SMART MRI in people with MS. We studied the correlation between SMART MPF metric and clinical test results in 33 MS patients. Furthermore, we investigate the ability of SMART MRI metrics to differentiate relapsing-remitting MS (RRMS) from progressive non-relapsing MS (PMS), as well as its correlation with biopsy-proven inflammatory demyelination.

Materials and Methods

Subjects

All studies were approved by the Washington University Institutional Review Board. Twenty healthy controls and 33 people with MS with relapsing-remitting MS (RRMS, $n = 11$), and progressive ($n = 22$) MS (PMS) clinical courses were enrolled after providing informed consent. Of the 22 PMS subjects, four were primary-progressive MS (mean EDSS = 5.6) and 18 were secondary-progressive MS (mean EDSS = 5.8). PMS subjects were progressing in absence of inflammatory disease activity (that is, no clinical relapses or Gd + lesions) within 24 months prior to enrollment.[26] For comparisons between relapsing and progressive, non-active MS, the PMS subjects were selected to be progressive without superimposed relapses or gadolinium-enhancing lesions within 24 months of entry. Demographic and clinical test information on the study subjects is shown in Table 1.

An additional study subject, a 35-year-old right-handed man who presented with right homonymous hemianopia and aphasia and who underwent CNS biopsy, provided imaging correlations of inflammatory demyelination with neuropathology. Clinical MRI demonstrated a large contrast-enhancing left parieto-occipital lesion with mass effect on the posterior horn of the left lateral ventricle. Because of continued enlargement of the lesion and worsening clinical course despite empiric high dose corticosteroids, a brain biopsy was performed. The biopsy showed inflammatory demyelination with axon sparing; the man was eventually diagnosed as having MS. Detailed information regarding this patient is provided in a previous publication.[30]

Clinical testing

For the 33 people with MS, Expanded Disability Status Scale (EDSS) and the Multiple Sclerosis Functional Composite (MSFC) along with its three components of 25-foot timed walk (25FTW) assessment of gait, nine-hole peg test (9HPT) assessment of upper extremity function, and paced auditory serial addition test (PASAT) assessment of cognitive function, as well as the symbol digit modalities test (SDMT) were all performed on the day of the MRI, by examiners blinded to imaging results. For analyses, the 25FTW and 9HPT were converted to *Z*-scores according to the MSFC Manual.[31]

Table 1. Demographic and clinical information of healthy controls and MS subjects.

		Healthy Control	RRMS	PMS	Normative data (Reference)
Number		20	11	22	
Mean Age $\pm$ SD (years)		40.1 $\pm$ 24	58.1 $\pm$ 6.9	55.3 $\pm$ 7.7	
(range)		(22–86)	(42–70)	(33–70)	
Female/Male		12/8	11/0	14/8	
EDSS mean $\pm$ SD		N/A	2.4 $\pm$ 1.1	5.8 $\pm$ 1.5	0
(range)			(1–4.5)	(2.5–8)	
25FTW mean $\pm$ SD (second) (range)		N/A	4.5 $\pm$ 0.6	48.5.0 $\pm$ 67.6	<5[27]
			(3.3–5.3)	(3.6–165.8)	
9HPT mean $\pm$ SD (second)	Dominant	N/A	22.9 $\pm$ 7.7	101.2 $\pm$ 219.2	<22[28]
(range)			(18.0–45.0)	(19.3–777)	
	Non-dominant	N/A	22.18 $\pm$ 3.7	135.8 $\pm$ 261.1	
			(16.6–31.8)	(22.8–777)	
SDMT mean $\pm$ SD		N/A	56.5 $\pm$ 9.1	44.3 $\pm$ 13.3	62.1 $\pm$ 10.7[29]
(range)			(49–80)	(12–60)	
3 sec PASAT mean $\pm$ SD		N/A	46.8 $\pm$ 10.9	43.6 $\pm$ 12.6	49.7 $\pm$ 9.8[29]
(range)			(28–58)	(15–59)	
2 sec PASAT mean $\pm$ SD		N/A	35.2 $\pm$ 11	32.7 $\pm$ 12.6	37.6 $\pm$ 9.5[29]
(range)			(25–55)	(7–51)	
Lesion volume/mm^3		N/A	3835 $\pm$ 3939	6518 $\pm$ 5403	N/A
			(229–14057)	(356–15825)	

One RRMS and two PMS subjects were left-handed. The rest were right-handed.

MRI

MRI data were collected using a 3T Trio scanner (Siemens, Erlangen, Germany) equipped with a 32-channel phased-array head coil. SMART data of voxel size 1mm^3 were acquired using three-dimensional multi-gradient-echo sequences with five flip angles α (5°, 10°, 20°, 40°, 60°) and three gradient echoes (echo times 2.3, 6.2, 10.1 ms) for each α. Generalized autocalibrating partially parallel acquisitions algorithm (GRAPPA)[32] with an acceleration factor of two and 24 autocalibrating lines in each phase encoding direction was used. The scan time for SMART MRI was 13 min 40 s (2 min 44 s per flip angle). The SMART data for healthy control and the patient who underwent biopsy were collected in approximately 9 min with voxel size 1.3 × 1.3 × 1.3 mm^3 (other parameters were kept the same), and subsequently reconstructed to 1 mm^3.

A phase-based B1 mapping technique accounting for effects of imperfect radio frequency spoiling and magnetization relaxation were implemented,[33] which required 2 min scan time. Standard clinical magnetization-prepared rapid gradient-echo (MPRAGE) images with voxel size 1 mm^3 were collected for segmentation purposes. Fluid-attenuated inversion recovery (FLAIR) images with voxel size of 1 × 1 × 3 mm^3 was used for outlining white matter lesions.

Image processing and segmentation

The multi-channel MRI data were combined using a published algorithm.[34] The combined data were then analyzed using the SMART model by accounting for the cross-relaxation effects between "free" and "bound" pools.[25] The derivation of the relationship between MPF and SMART metrics is presented in the Supplementary Material.

Brain gray and white matter segmentation was performed on MPRAGE images using FreeSurfer 5.3.0 (Martinos Center for Biomedical Imaging, MGH/HST, US) with visual inspection of each segmented region of interest (ROI) for accuracy. 68 cortical gray matter and 68 corresponding subcortical white matter ROIs (34 each per hemisphere) were generated. Global gray matter and white matter masks in each hemisphere were generated by combining 34 ROIs in gray matter and white matter in each hemisphere. Using FSL 5.0.0 software (Analysis Group, FMRIB, Oxford, UK), MPRAGE images were then co-registered with SMART images corresponding to flip angle 20° and TE = 2.3 ms (that was also used as the reference for co-registration of SMART data with other flip angles). This procedure also co-registered ROIs generated by FreeSurfer to all SMART metrics maps. To minimize partial volume effects, CSF masks were generated using FSL based on the SMART images with flip angle 20° and TE = 2.3 ms. Applying regional and CSF masks, SMART

metrics for each ROI in normal-appearing cortical gray matter (NAGM), normal-appearing subcortical white matter (NAWM), defined as tissues outside of focal white matter lesions, were calculated using the median values to reduce outlier effects. White matter lesion masks were obtained using "lesion-TOADS" tool[35] in Medical Image Processing, Analysis and Visualization software[36] using both MPRAGE and FLAIR images co-registered with FSL. White matter lesion masks were visually inspected to ensure accuracy. For each MS subject, median values of SMART metrics in their lesions were computed.

Statistical analysis

For 33 MS patients, SMART metrics in cortical NAGM, subcortical NAWM, and lesions were examined for correlations with EDSS, MSFC (also individually for 25FTW, 9HPT, and PASAT components of the MSFC), and SDMT. One PMS subject was excluded from analysis due to image artifacts precluding accurate measurements. Thus, 21 out of 22 PMS subjects were used for subsequent imaging analysis. Statistical program R was used for data analysis. Spearman rank test was used to compute rho values, with age and gender as covariates. As a non-parametric test, Spearman rank correlation minimizes bias from outliers in clinical measurements. Two-sample *t*-test was used to compare group differences based on SMART measurements. False discovery rate was used to adjust for multiple comparisons.

Results

Examples of axial SMART images corresponding to MPF and other SMART metrics, as well as an axial FLAIR image and an axial MPRAGE image for a subject with PMS are shown in Figure 1. In panel (a), red arrows indicate regions of reduced MPF. Reduced signal on $R1$, $R1_f$, and MPRAGE images (seen as hypointense signals of a focal lesion on $R1$, $R1_f$, and MPRAGE images), and the hyperintense signals on proton density (S_0) and FLAIR images indicated tissue abnormalities. Although these changes are not pathologically specific, the abnormalities were consistent with reduced myelin content (Fig. 1). In addition, our data showed that SMART-derived MPF was repeatable between two scans in a subgroup of five patients in the MS cohort (Fig. S1).

Group differences in MPF

MPF was significant higher in the healthy group than in subjects with MS. In both left and right hemispheres of NAGM and NAWM, MPF differentiated RRMS from non-relapsing PMS cohorts at the group level, although considerable overlap of individual subjects between the two MS subgroups was seen (Fig. 2). In particular, MPF of left hemisphere subcortical NAWM was best able to distinguish among the controls and two MS subtypes at the group level (Fig. 2C). The median value of MPF in MS lesions also distinguished the RRMS cohort from the PMS cohort, with RRMS having higher median lesion MPF than PMS (Fig. 2E). In contrast, lesion volume measurements did not distinguish the two MS groups (Fig. 2F). No significant or trends for differences in MPF measurements between male and female PMS subjects were found (Fig. S2).

Region-wise analysis showed that SMART MPF measurements in subcortical NAWM of were universally higher than in cortical NAGM, supporting the contention that MPF reflects myelination (Fig. 3; Fig. S3). The HC group had higher MPF than the two MS cohorts. In addition, the RRMS cohort had higher MPF measurements than the PMS cohort, in both NAGM and NAWM. The right hemisphere showed similar results to the left hemisphere (Fig. S3).

Clinical correlations

NAWM and NAGM are often not truly normal in MS brain tissues.[7] SMART MPF measurements of NAWM and NAGM of both hemispheres correlated with motor-related clinical test scores (Table 2). MPF measurements in subcortical NAWM demonstrated stronger correlations with clinical test scores than MPF in cortical NAGM. Median values of MPF in the MS lesions showed significant correlations with EDSS ($p < 0.001$), 25FTW ($p < 0.001$), 9HPT (Dominant) ($p = 0.002$), 9HPT (Non-dominant) ($p = 0.002$), and MSFC ($p = 0.013$), whereas lesion volume did not show significant correlations with any clinical scores (Table 3). Quantitative $R1$ metric showed significant correlations only with the PASAT for NAGM (r = 0.46, $p = 0.004$) and for NAWM (r = 0.38, $p = 0.025$) (Table S1). In both NAWM and NAGM, MPF metrics of the left hemisphere showed stronger correlations with clinical assessments than MPF metrics of the right hemisphere. This was true even for left hemisphere correlations of 9HPT with the ipsilateral left hand in right-hand dominant subjects (Table 2, Fig. 4).

Since global MPF measurements correlated with clinical tests, MPF was next investigated in region-wise analysis. Regional MPF in the left hemisphere of right-handed subjects showed consistently stronger correlations with MSFC and its component 9HPT than MPF in the right hemisphere (Figs. 4, 5). Additionally, in most of the ROIs, MPF in NAWM demonstrated stronger correlations with clinical test scores than did MPF in NAGM. Cortical myelin distribution of healthy controls measured by MPF
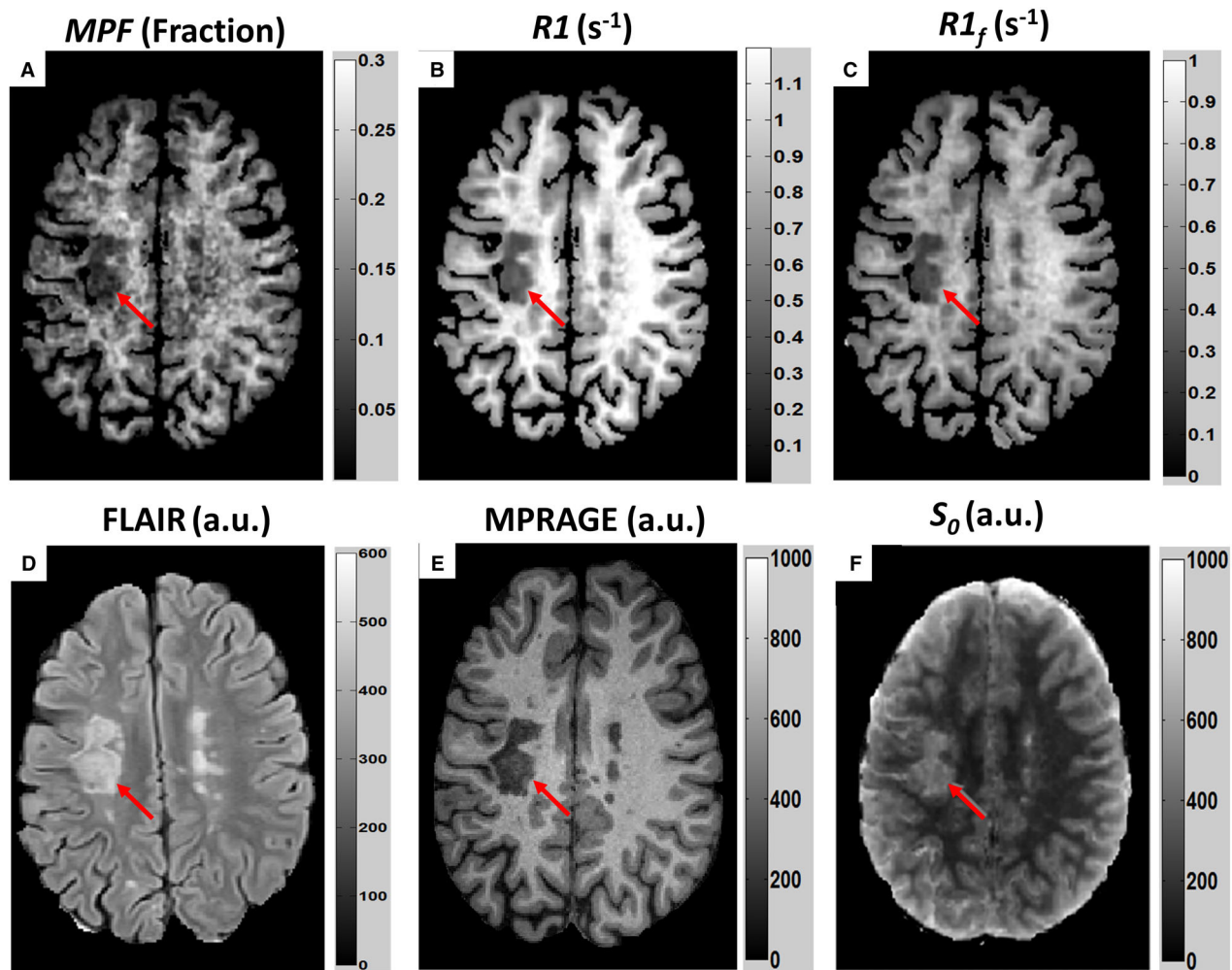
Figure 1. Examples of axial SMART metrics images alongside axial FLAIR and MPRAGE images. Macromolecule proton fraction (MPF) [units range from 0 (no bound protons) to 1 (no free protons)] (A), $R1$ (1/s) (B), $R1_f$ (the longitudinal relaxation rate of the free pool), (C), FLAIR (a.u.) (D), MPRAGE (a.u.) (1/s) (E) and S_0 (a.u.) (F) images were obtained from a 34 year-old man with MS since age 16, now with non-relapsing secondary progressive MS (EDSS 7.5). One focal lesion is indicated by a red arrow. MPF images, as well as $R1$, $R1_f$, and MPRAGE images, showed hypointense (reduced) signals at sites of lesions. Proton density (S_0) and FLAIR showed hyperintense signals at sites of lesions. SMART images do not exactly match FLAIR due to different slice thicknesses (1 mm for SMART and 3 mm for FLAIR). a.u. = arbitrary units. Note that the major advantage of SMART is not in detecting lesions but in quantitative assessment of tissue damage in normal-appearing tissue as presented in Table 2 and Figure 2.

showed the primary sensory and motor regions to be more myelinated than other regions (Fig. S4), in agreement with previous studies.[37]

Longitudinal analysis in a biopsied patient who was eventually diagnosed as MS

The SMART MRI was applied to a patient who underwent biopsy, with histopathological confirmation of inflammatory demyelination.[30] Two weeks following biopsy, the patient underwent imaging with SMART technique. This revealed significantly lower MPF in lesion versus contralateral normal white matter area of similar size ($p < 10^{-10}$, Fig. 6D,F). After 6 months, qualitative FLAIR images showed the reduced size of the left parieto-occipital hyperintensity (Fig. 6A,B). MPF images of each visit show the parieto-occipital lesion and abnormal left optic radiation (blue arrows in Fig. 6D,E). At Visit 2, MPF of the lesion was significantly lower than in the contralateral normal-appearing region of white matter (Fig. 6F, $p < 10^{-10}$), but the MPF in the lesion was significantly higher at Visit 2 than at visit 1($p < 10^{-10}$). Though still abnormal, MPF values in the lesion at Visit 2 had partially normalized, suggesting partial recovery of
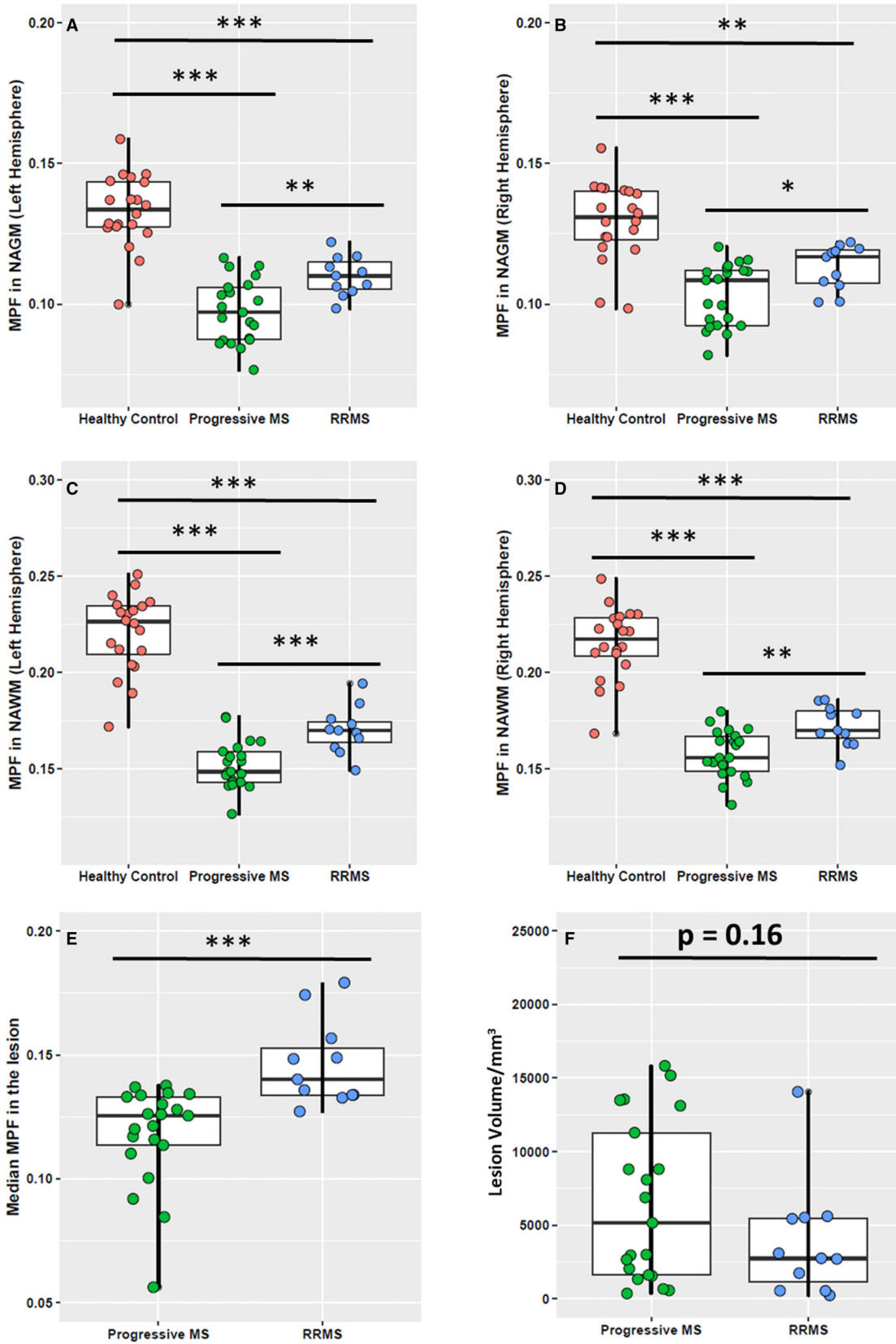
Figure 2. Group comparisons based on macromolecule proton fraction (MPF) measurements in cortical NAGM (A, B), subcortical NAWM (C, D) and lesion (E), and lesion volume(F). Healthy control subjects displayed higher MPF than subjects with MS, with the RRMS group higher than the non-relapsing PMS group. In both gray and white matter, MPF of the left hemisphere differentiated the two MS subtypes better than MPF of the right hemisphere. Median value of MPF in the lesion revealed higher MPF in the RRMS group than the progressive MS group. Lesion volume measurement did not distinguish the two MS groups. Boxes represent the interquartile ranges; the horizontal lines within the boxes are median values. In graph (A–D), points are median values of normal-appearing tissue in individual subjects. In graph (E), points are median values of MPF in the lesions of each individual subject. In graph (F), points are lesion volume measurements of each MS subject. *** $p < 0.001$, ** $p < 0.01$, * $p < 0.05$. p values were determined after adjusting for multiple comparisons using false discovery rate.

tissue damage in agreement with the patient's improving clinical performance at Visit 2.

Discussion

Improved and quantitative imaging biomarkers that readily assess MS tissue damage and repair, including in areas that appear normal on conventional MRI, are needed for disease monitoring and putative reparative treatments development.[38] The recently developed SMART MRI technique can generate the MPF which reflects the level of myelination. Here, for the first time, we applied SMART MRI in patients with RRMS and PMS to investigate associations of quantitative SMART MPF metric with the different MS subtypes and physical and cognitive disease severity.

In this study, SMART MPF showed significant correlations with motor-related clinical test scores at both global and regional levels. We found lower MPF derived via SMART MRI in MS lesions than in normal-appearing tissues, in agreement with previous reports of hypointense MPF derived via qMT signals in demyelinated and dysmyelinated CNS tissue.[16,39] Values of MPF observed in this study were in general agreement with published studies.[18,40] The left and the right hemispheres were analyzed separately in our patient cohorts to explore hemispheric differences. We observed stronger associations between clinical measures and the MPF values in the left hemisphere. This was not unexpected as the left cerebral hemisphere is reported to have a strong involvement in complex motor control for both right- and left-handed people, an effect that is due to hemispheric specialization rather than handedness.[41,42] In addition, disrupting the left premotor cortex by transcranial magnetic stimulation was reported to result in longer reaction times than right premotor cortex in response selection, regardless of handedness.[43–45] Published studies and our data support the idea that tissue damage in the left hemisphere plays a key role in bilateral motor function.

We found that MPF readily differentiated healthy brains from those with MS, but importantly also separated the RRMS from the non-relapsing PMS groups. Patients in the two MS subgroups were specifically chosen to be of very similar ages, to remove the confound of age.

Separation between PMS and RRMS was noted in almost all ROIs. Lower SMART MPF was observed for both global (entire cerebral cortical NAGM and subcortical NAWM) and region-wise measurements in PMS versus RRMS. This result is in agreement with published studies showing worse pathology, including greater myelin loss, in progressive than RRMS patients.[7,46] Although lesion volumes are sometimes used to differentiate subtypes of MS, it is notable that lesion volumes failed to differentiate RRMS from non-relapsing PMS patients. Non-active PMS is a subgroup for whom highly effective treatments are lacking. The quantitative delineation of PMS from similar-aged RRMS patients by SMART MPF is an important finding because it suggests that SMART MPF can potentially measure the pathology associated with progressive disease which is thought to involve widespread diffuse damage of the NAWM and NAGM in the brains of those with progressive MS.[47]

Our longitudinal assessment of a patient with a demyelinating lesion showed an initial significant MPF reduction in the left optic radiation affected by the histopathologically confirmed demyelinating lesion (with relative axonal sparing).[30] Six months later, increasing MPF was found in the lesion in concert with clinical improvement in the patient. These longitudinal data indicate the potential ability of SMART MPF to be a quantitative outcome measure in trials of remyelinating/reparative agents.

The MPF metric derived from qMT is a quantitative proxy reflecting myelin content.[21,22] Using multi-gradient-echo sequence, we developed SMART MRI to generate a qMT-like measure (SMART MPF). Like qMT, SMART MRI measures MPF by assessing the exchange between "free" and "bound" pools. A major advantage of the SMART technique is that it does not require high energy deposition, especially important for high field MRI scanners. Data in this study were derived from a high resolution (1 mm^3) SMART protocol and were acquired within a clinically feasible scan time (16 min, including B1 mapping).

This study has a few limitations. The RRMS group was smaller than the progressive MS group. This is because the RRMS subjects in the study were specifically chosen to be of similar age to the progressive MS patients, and
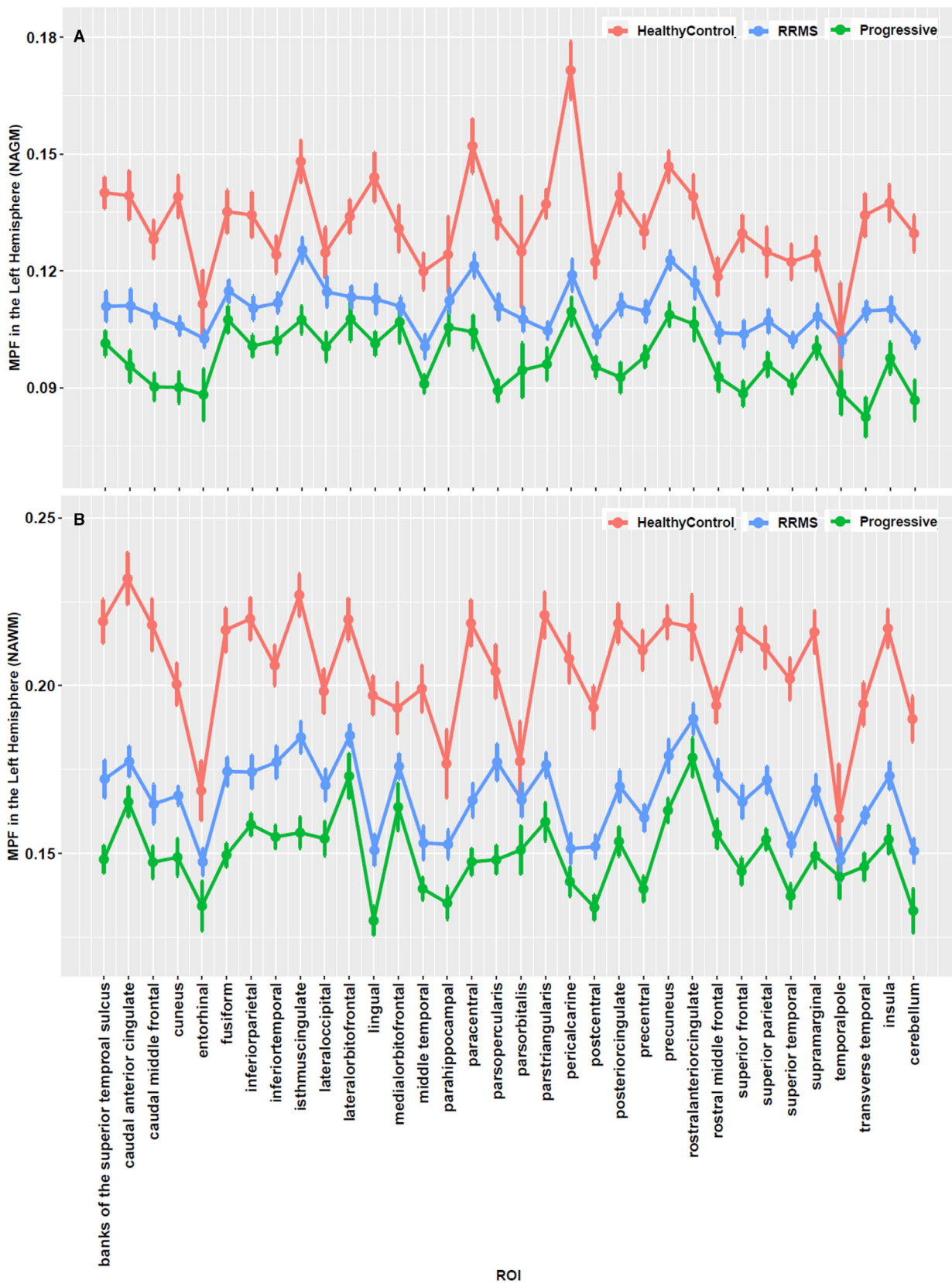
Figure 3. Regional macromolecule proton fraction (MPF) of the left hemisphere revealed MPF as consistently highest in the healthy control group and consistently lowest in the PMS cohort in cortical NAGM (B) and subcortical NAWM (A). Median values of MPF measurements of each cortical/subcortical ROI in the left hemisphere for each clinical subtype are plotted. Error bars are the standard error of MPF measurement. MPF in NAWM ROIs were significantly higher than MPF in NAGM, consistent with the greater myelin content in white matter than gray matter. The right hemisphere showed similar results to the left hemisphere (Fig. S3).

Table 2. Macromolecule proton fraction (MPF) in the cortical NAGM and subcortical NAWM correlated with clinical assessments.

	MPF in NAGM				MPF in NAWM			
	Left hemisphere		Right hemisphere		Left hemisphere		Right hemisphere	
	rho	p	rho	p	rho	p	rho	p
EDSS	−0.360	0.009	−0.251	0.070	−0.491	<0.001	−0.314	0.022
25FTW	−0.334	0.015	−0.288	0.034	−0.404	0.003	−0.315	0.022
9HPT(Dominant)	0.554	<0.001	0.499	<0.001	0.600	<0.001	0.461	0.001
9HPT(Non-dominant)	0.521	<0.001	0.439	0.002	0.650	<0.001	0.462	0.001
PASAT(2S)	0.067	0.654	0.086	0.570	0.256	0.068	0.223	0.103
PASAT(3S)	−0.029	0.820	0.033	0.820	0.149	0.309	0.106	0.473
SDMT	0.136	0.366	0.235	0.095	0.313	0.023	0.249	0.071
MSFC	0.398	0.003	0.359	0.009	0.525	<0.001	0.407	0.003

MPF measurements in both NAGM and NAWM correlated with assessments related to motor function. NAWM MPF had stronger correlations with clinical tests than NAGM MPF. The MPF in left hemisphere demonstrated a stronger correlation with clinical scores than did MPF in the right hemisphere. MPF of NAWM in left hemisphere correlated modestly with the SDMT measure of cognition. For 9HPT, the three MS subjects who were left-handed were not included in analyses. 9HPT and 25FTW results were converted to Z score based on MSFC. Spearman rho and p values were computed in R, with age and gender as covariates. Spearman rank correlation was used to minimize the bias from outliers in clinical scores. All listed p values are after multiple comparison correction using false discovery rate.

Table 3. Median macromolecule protein fraction (MPF) in MS lesions shows significant correlations with motor-related clinical assessments.

	Median MPF in the lesion		Median $R1$ in the lesion/s^{-1}		Lesion Volume/mm^3	
	rho	p	rho	p	rho	p
EDSS	−0.511	<0.001	−0.320	0.030	0.241	0.090
25FTW	−0.538	<0.001	−0.425	0.002	0.237	0.090
9HPT(Dominant)	0.437	0.002	0.234	0.090	−0.183	0.230
9HPT(Non-dominant)	0.443	0.002	0.299	0.042	−0.110	0.484
PASAT(2S)	−0.248	0.090	−0.032	0.863	0.045	0.808
PASAT(3S)	−0.263	0.090	−0.021	0.892	−0.032	0.863
SDMT	0.121	0.395	0.310	0.030	−0.259	0.090
MSFC	0.362	0.013	0.239	0.090	−0.135	0.395

Median $R1$ was correlated with EDSS, 25 foot-timed walk, 9-hole peg test, and with the SDMT cognitive test. Lesion volume did not show significant correlations with clinical scores. Spearman rho and p values were computed in R, with age and gender as covariates. All listed p values are after multiple comparison correction using false discovery rate.

fewer RRMS subjects of older age were identified for recruitment. The RRMS group was also all female. In the biopsied patient, reduced MPF was in agreement with the demyelination and axonal sparing seen by histology, but could also be due to other types of damage and to edema. However, edema would not likely be a major factor after 6 months of recovery when MPF was still reduced in the lesion. Although the patient who underwent biopsy was eventually diagnosed as MS, the demyelinating lesion analyzed in this case was different from typical MS lesions in

that it was larger with more surrounding edema, concerning for a tumor. Additional histo-pathological validation of the SMART technique is still needed. In addition, the current SMART technique did not consider the distribution of T2 within the bound pool, which will be addressed in future studies. Comparison of SMART MRI to other imaging techniques that are sensitive to myelin content will be investigated in upcoming studies.

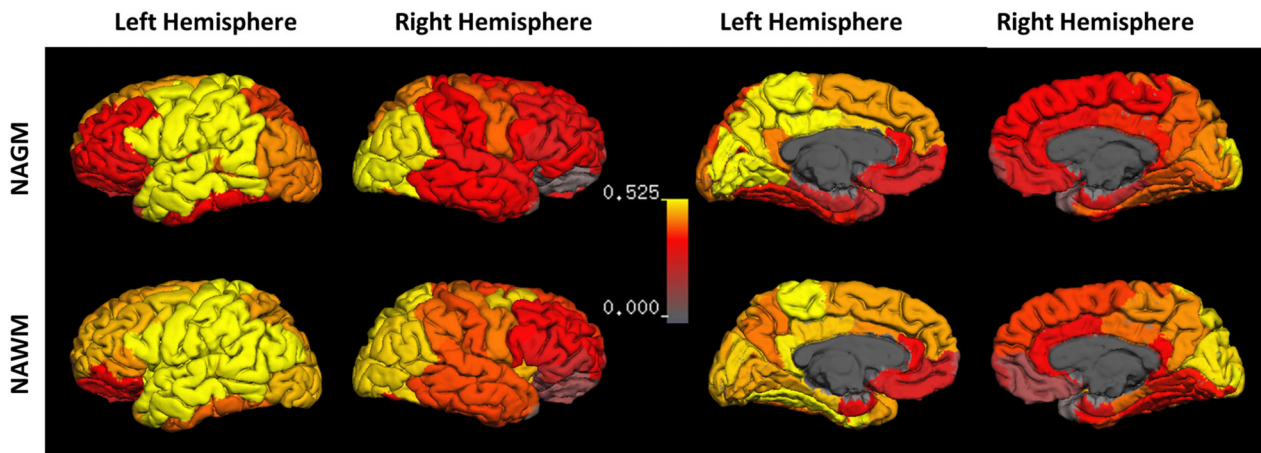In summary, SMART MPF provides information similar to that provided by qMT, without radio frequency

Figure 4. Macromolecule proton fraction (MPF) correlations with 9-hole peg test. MPF in NAGM (first row) and subcortical NAWM (second row) of the dominant left hemisphere correlated better than the right hemisphere with 9-hole peg test results of the non-dominant left hand. Data from the three left-handed subjects were not included in the correlation analysis to ensure all subjects had the same dominant hemisphere. Interestingly, stronger correlations were noted between the left-hand 9-HPT results and the ipsilateral MPF in the dominant left hemisphere motor regions than for the same regions in the contralateral right hemisphere. More extensive and stronger correlations were noted for NAWM than NAGM. Color bar: Scale of Spearman rho values.
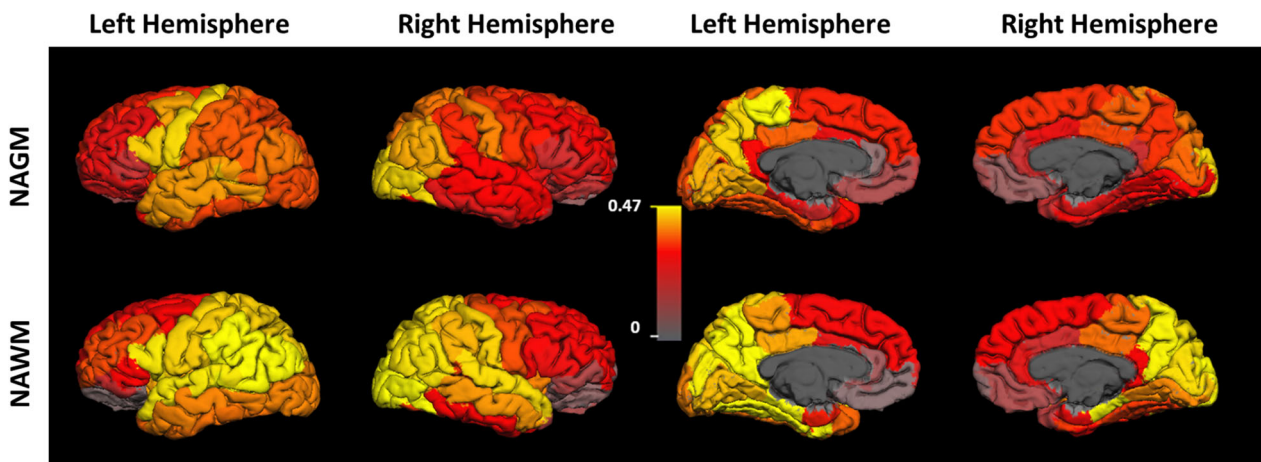

Figure 5. Correlations of MPF with MSFC scores. MPF in subcortical NAGM (first row) correlated better with MSFC than cortical NAWM (second row). All MS subjects were included in this correlation analysis. No clear differences between hemispheres were noted. Color bar: Scale of Spearman rho values.

energy restrictions. Thus, SMART MRI might be used to assess demyelination and remyelination in MS and related diseases. Based on these attributes, SMART MPF has a potential to be used as a quantitative non-invasive outcome measure in future clinical trials of putative remyelinating agents.

Author Contributions

Anne H. Cross, Dmitriy A. Yablonskiy, and Biao Xiang designed the study, supervised the experiments, and wrote

the manuscript. Anne H. Cross, Dmitriy A. Yablonskiy, Biao Xiang, Jie Wen, Daniel Mamah, Alexander L. Sukstanskii, and Robert E. Schmidt performed the experimental work and/or its analysis, and refined the manuscript.
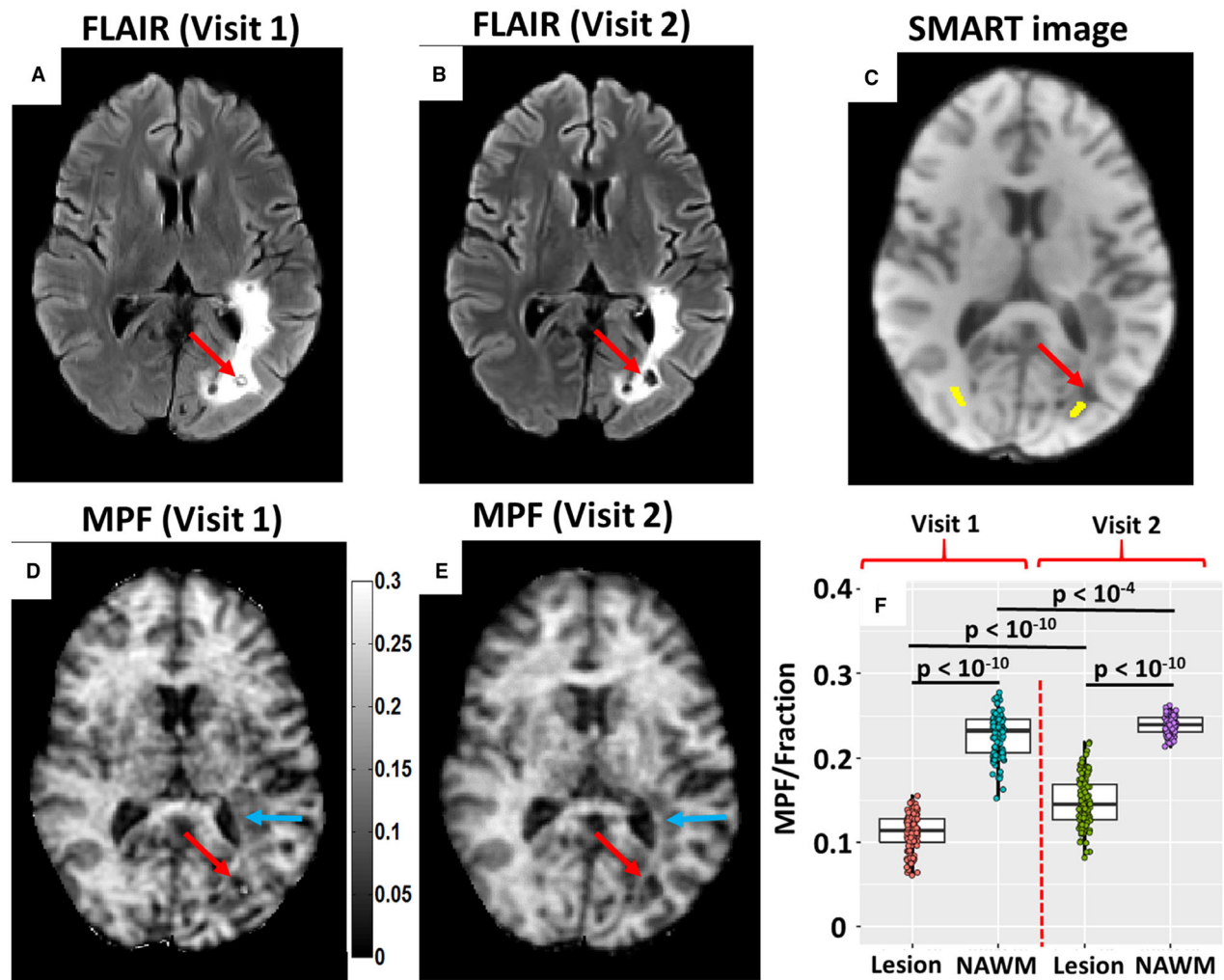
Figure 6. Longitudinal macromolecule protein fraction (MPF) measurements in biopsied inflammatory demyelinating lesion. Data were obtained 2 weeks and 6 months after biopsy of a tumefactive left hemisphere lesion in a 35 year old man. MRI images in Visit 1 and Visit 2 are coregistered. (A), (B) FLAIR images show a large left parieto-occipital hyperintense lesion on both visits with smaller size of hyperintensity at Visit 2 compared with Visit 1. Red arrows indicate the biopsy site. (C) SMART image corresponding to the first echo of flip angle 20° show a ROI (marked in yellow) used for the SMART analyses of the biopsied lesion and a comparable ROI in NAWM of the contralateral normal-appearing side, for comparison. (D), (E) MPF images of Visit 1 and Visit 2 show the parieto-occipital lesion and abnormal left optic radiation (blue arrows). The demyelinated lesion in the left optic radiation was consistent with right homonymous hemianopia on examination. (F) Group comparison between ROIs in the lesion and NAWM based on MPF. For each visit, MPF in the lesion was substantially lower than in contralateral NAWM with little overlap. MPF values in the lesion at Visit 2, though still abnormal, had become more normal, suggesting incomplete recovery, in agreement with the improved clinical examination at Visit 2.

Conflict of Interest

Dr. Anne Cross reports personal fees from Biogen, Celgene, EMD Serono, Genentech/Roche, Novartis, TG Therapeutics, Horizon Pharma, Greenwich Biosciences, Bristol Myers Squibb, and Janssen, and grants from EMD Serono and from Genentech/Roche, outside the submitted work. Other authors have no competing interests, financial or otherwise.

References

1. Wallin MT, Culpepper WJ, Campbell JD, et al. The prevalence of MS in the United States. A population-based estimate using health claims data. Neurology. 2019;92(10):e1029-e1040.

2. McDonald WI, Compston A, Edan G, et al. Recommended diagnostic criteria for multiple sclerosis: guidelines from the International Panel on the diagnosis of multiple sclerosis. Ann Neurol. 2001;50(1):121-127.

3. Brex PA, Ciccarelli O, O'Riordan JI, Sailer M, Thompson AJ, Miller DH. A longitudinal study of abnormalities on MRI and disability from multiple sclerosis. N Engl J Med. 2002;346(3):158-164.

4. Dalton CM, Brex PA, Miszkiel KA, et al. New T2 lesions enable an earlier diagnosis of multiple sclerosis in clinically isolated syndromes. Ann Neurol. 2003;53(5):673-676.

5. McFarland HF, Barkhof F, Antel J, Miller DH. The role of MRI as a surrogate outcome measure in multiple sclerosis. Mult Scler J. 2002;8(1):40-51.

6. Jakimovski D, Ramasamy DP, Zivadinov R. Magnetic resonance imaging and analysis in multiple sclerosis. In: Rizvi SA, Cahill JF, Coyle PK, eds. Clinical Neuroimmunology: Multiple Sclerosis and Related Disorders. Springer International Publishing; 2020:109-136.

7. Kutzelnigg A, Lucchinetti CF, Stadelmann C, et al. Cortical demyelination and diffuse white matter injury in multiple sclerosis. Brain. 2005;128(Pt 11):2705-2712.

8. Laule C, Vavasour IM, Kolind SH, et al. Magnetic resonance imaging of myelin. Neurotherapeutics. 2007;4 (3):460-484.

9. Horsfield MA. Magnetization Transfer Imaging in Multiple Sclerosis. J Neuroimaging. 2005;15(s4):58S-67S.

10. Filippi M, Agosta F. Magnetization transfer MRI in multiple sclerosis. J Neuroimaging. 2007;17(Suppl 1):22S-26S.

11. Schmierer K, Scaravilli F, Altmann DR, Barker GJ, Miller DH. Magnetization transfer ratio and myelin in postmortem multiple sclerosis brain. Ann Neurol. 2004;56 (3):407-415.

12. Sled JG, Pike GB. Quantitative imaging of magnetization transfer exchange and relaxation properties in vivo using MRI. Magn Reson Med. 2001 Nov;46(5):923-931.

13. Tozer D, Ramani A, Barker GJ, Davies GR, Miller DH, Tofts PS. Quantitative magnetization transfer mapping of bound protons in multiple sclerosis. Magn Reson Med. 2003;50(1):83-91.

14. Stanisz GJ, Odrobina EE, Pun J, et al. T1, T2 relaxation and magnetization transfer in tissue at 3T. Magn Reson Med. 2005;54(3):507-512.

15. Soellinger M, Langkammer C, Seifert-Held T, Fazekas F, Ropele S. Fast bound pool fraction mapping using stimulated echoes. Magn Reson Med. 2011;66(3):717-724.

16. Yarnykh VL, Bowen JD, Samsonov A, et al. Fast whole-brain three-dimensional macromolecular proton fraction mapping in multiple sclerosis. Radiology. 2015;274(1):210-220.

17. van Gelderen P, Jiang X, Duyn JH. Rapid measurement of brain macromolecular proton fraction with transient saturation transfer MRI. Magn Reson Med. 2017 Jun;77 (6):2174-2185.

18. West KL, Kelm ND, Carson RP, Gochberg DF, Ess KC, Does MD. Myelin volume fraction imaging with MRI. Neuroimage. 2018;182:511-521.

19. Hou J, Wong VW-S, Jiang B, et al. Macromolecular proton fraction mapping based on spin-lock magnetic resonance imaging. Magn Reson Med. 2020;84:3157-3171.

20. Kisel AA, Naumova AV, Yarnykh VL. Macromolecular proton fraction as a myelin biomarker: principles, validation, and applications. Front Neurosci. 2022;16:2022-February-09;16.

21. Schmierer K, Tozer DJ, Scaravilli F, et al. Quantitative magnetization transfer imaging in postmortem multiple sclerosis brain. J Magn Reson Imaging. 2007;26(1):41-51.

22. Underhill HR, Rostomily RC, Mikheev AM, Yuan C, Yarnykh VL. Fast bound pool fraction imaging of the in vivo rat brain: association with myelin content and validation in the C6 glioma model. Neuroimage. 2011;54 (3):2052-2065.

23. Dortch RD, Bagnato F, Gochberg DF, Gore JC, Smith SA. Optimization of selective inversion recovery magnetization transfer imaging for macromolecular content mapping in the human brain. Magn Reson Med. 2018;80(5):1824-1835.

24. Battiston M, Schneider T, Grussu F, et al. Fast bound pool fraction mapping via steady-state magnetization transfer saturation using single-shot EPI. Magn Reson Med. 2019;82(3):1025-1040.

25. Sukstanskii AL, Wen J, Cross AH, Yablonskiy DA. Simultaneous multi-angular relaxometry of tissue with MRI (SMART MRI): theoretical background and proof of concept. Magn Reson Med. 2016 Mar;15(77):1296-1306.

26. Lublin FD, Reingold SC, Cohen JA, et al. Defining the clinical course of multiple sclerosis: the 2013 revisions. Neurology. 2014;83(3):278-286.

27. Kaufman M, Moyer D, Norton J. The significant change for the Timed 25-foot Walk in the multiple sclerosis functional composite. Mult Scler. 2000;6(4):286-290.

28. Oxford Grice K, Vogel KA, Le V, Mitchell A, Muniz S, Vollmer MA. Adult norms for a commercially available Nine Hole Peg Test for finger dexterity. Am J Occup Ther. 2003;57(5):570-573.

29. Strober L, Englert J, Munschauer F, Weinstock-Guttman B, Rao S, Benedict RH. Sensitivity of conventional memory tests in multiple sclerosis: comparing the Rao Brief Repeatable Neuropsychological Battery and the

Minimal Assessment of Cognitive Function in MS. Mult Scler. 2009;15(9):1077-1084.

30. Xiang B, Wen J, Lu H-C, Schmidt RE, Yablonskiy DA, Cross AH. In vivo evolution of biopsy-proven inflammatory demyelination quantified by R2t* mapping Ann Clin Transl Neurol 2020;7:1055–60, 1060.

31. Fischer JS, Rudick RA, Cutter GR, Reingold SC. The Multiple Sclerosis Functional Composite Measure (MSFC): an integrated approach to MS clinical outcome assessment. National MS Society Clinical Outcomes Assessment Task Force. Mult Scler. 1999;5(4):244-250.

32. Griswold MA, Jakob PM, Heidemann RM, et al. Generalized autocalibrating partially parallel acquisitions (GRAPPA). Magn Reson Med. 2002;47(6):1202-1210.

33. Wen J, Sukstanskii AL, Yablonskiy DA. Phase-sensitive B1 mapping: effects of relaxation and RF spoiling. Magn Reson Med. 2018;80(1):101-111.

34. Luo J, Jagadeesan BD, Cross AH, Yablonskiy DA. Gradient echo plural contrast imaging--signal model and derived contrasts: T2*, T1, phase, SWI, T1f, FST2*and T2*-SWI. Neuroimage. 2012;60(2):1073-1082.

35. Shiee N, Bazin PL, Ozturk A, Reich DS, Calabresi PA, Pham DL. A topology-preserving approach to the segmentation of brain images with multiple sclerosis lesions. Neuroimage. 2010;49(2):1524-1535.

36. McAuliffe MJ, Lalonde FM, McGarry D, Gandler W, Csaky K, Trus BL, editors. Medical Image Processing, Analysis and Visualization in Clinical Research. Computer-Based Medical Systems, 2001 CBMS 2001 Proceedings 14th IEEE Symposium on 2001. Institute of Electrical and Electronics Engineers (IEEE); 2001.

37. Nieuwenhuys R, Broere CA. A map of the human neocortex showing the estimated overall myelin content of the individual architectonic areas based on the studies of Adolf Hopf. Brain Struct Funct. 2017;222:465-480.

38. Oh J, Ontaneda D, Azevedo C, et al. Imaging outcome measures of neuroprotection and repair in MS: a consensus statement from NAIMS. Neurology. 2019;92 (11):519-533.

39. Levesque IR, Giacomini PS, Narayanan S, et al. Quantitative magnetization transfer and myelin water imaging of the evolution of acute multiple sclerosis lesions. Magn Reson Med. 2010;63(3):633-640.

40. van Gelderen P, Duyn JH. White matter intercompartmental water exchange rates determined from detailed modeling of the myelin sheath. Magn Reson Med. 2018;81:628-638.

41. Kim SG, Ashe J, Hendrich K, et al. Functional magnetic resonance imaging of motor cortex: hemispheric asymmetry and handedness. Science. 1993;261(5121):615-617.

42. Verstynen T, Diedrichsen J, Albert N, Aparicio P, Ivry RB. Ipsilateral motor cortex activity during unimanual hand movements relates to task complexity. J Neurophysiol. 2005;93(3):1209-1222.

43. Schluter ND, Rushworth MF, Passingham RE, Mills KR. Temporary interference in human lateral premotor cortex suggests dominance for the selection of movements. A study using transcranial magnetic stimulation. Brain. 1998;121(Pt 5):785-799.

44. Rushworth MF, Johansen-Berg H, Göbel SM, Devlin JT. The left parietal and premotor cortices: motor attention and selection. Neuroimage. 2003;20(Suppl 1):S89-S100.

45. O'Shea J, Johansen-Berg H, Trief D, Göbel S, Rushworth MF. Functionally specific reorganization in human premotor cortex. Neuron. 2007;54(3):479-490.

46. Dutta R, Trapp BD. Relapsing and progressive forms of multiple sclerosis: insights from pathology. Curr Opin Neurol. 2014;27(3):271-278.

47. Absinta M, Lassmann H, Trapp BD. Mechanisms underlying progression in multiple sclerosis. Curr Opin Neurol. 2020;33(3):277-285.

Supporting Information

Additional supporting information may be found online in the Supporting Information section at the end of the article.

Figure S1 SMART-derived MPF measurement showed high repeatability in five MS subjects. The two scans were separated by 9 months. The Expanded Disability Status Scale (EDSS) of the five subjects remained the same between two scans. No significant changes of other clinical tests were observed. Paired-sample t-test was used to compare two scans.

Figure S2. Group comparisons based on macromolecule proton fraction (MPF) measurements in female and male PMS subjects. No significant difference between MPF measurements in male and female PMS subjects were found. Points are median values of normal-appearing tissue in individual subjects.

Figure S3. Regional macromolecule protein fraction (MPF) of the right hemisphere shows a consistent trend with healthy control highest and progressive MS cohort lowest in both cortical NAGM (b) and subcortical NAWM (a). Median values of MPF measurement of each cortical/subcortical ROI in the left hemisphere for each clinical subtype are plotted. Error bars are the standard error of MPF measurement. MPF in NAWM ROIs were significantly higher than MPF in NAGM, consistent with the greater myelin content in white matter.

Figure S4. Cortical myelin distribution of healthy controls measured by macromolecule proton fraction (MPF). The primary sensory and motor regions are more myelinated than other regions. Color bar: Scale of MPF values.

Table S1. Association between Global *R1* measurements in cortical NAGM and subcortical NAWM and clinical assessments. The only significant correlations for *R1* measurements are with the two second PASAT, a test of cognitive function test. For 9HPT, three left-handed subjects were removed to ensure all test subjects were right-handed. Spearman rho and p values were computed in R, with age and gender as covariates. All listed p values are after multiple comparison correction using false discovery rate. Statistically significant correlations are highlighted in yellow.[2]